DE GRUYTER OPEN

Chemical and Process Engineering 2015, 36 (3), 331-344
DOI: 10.1515/cpe-2015-0023

PAN POLSKA AKADEMIA NAUK

INTENSIFICATION OF HEAT TRANSFER BETWEEN HEAT EXCHANGE SURFACES AT LOW *RE* VALUES

Jozef Cernecky*, Zuzana Brodnianska, Jan Koniar

Technical University in Zvolen, Faculty of Environmental and Manufacturing Technology, Department of Environmental and Technology, Studentska 26, 960 53 Zvolen, Slovakia

This contribution deals with the heat transfer parameters and pressure losses in heat exchange sets with six geometrical arrangements at low *Re* values (*Re* from 476 to 2926). Geometrical arrangements were characterised by the *h*/*H* ratio ranging from 0.2 to 1.0. The experiments used the holographic interferometry method in real time. This method enables visible and quantitative evaluations of images of temperature fields in the examined heat exchange. These images are used to determine the local and mean heat transfer parameters. The obtained data were used to determine the *Colburn j-factor* and the friction coefficient *f*. The measured values show that by using the profiled heat exchange surfaces and inserting regulating tubes, an intensification of heat transfer (increase of Nu_m, and/or *j*) was achieved. However, pressure losses recorded a significant increase (increase of *f*).

Keywords: heat transfer, heat exchange surface, Colburn j-factor, interferometry

1. INTRODUCTION

Authors in various countries around the world have addressed the topic of heat transfer between shaped horizontal heat exchange surfaces. Such sets have many practical uses, such as heat exchange surfaces of plate heat exchangers, heating elements, cooling or heating devices and ribbed surfaces of engines, machines, technological equipment but also as ribbed surfaces of cooling parts in electrotechnical equipment. Several authors have used optical methods for the visualisation of temperature fields in the vicinity of shaped heated surfaces, so that the examined area is not disrupted by various sensors.

An overview of optical methods that can be used to research heat transfer has been provided by Hauf and Grigull (1970), who described the shadow and Schlieren methods, as well as the interference method with demonstrative examples. Kilicaslan and Sarac (1998) used the holographic interferometry method to determine the temperature fields and the Laser Doppler Anemometry method for the distribution of velocity. The study was performed on heat exchange surfaces with a triangular and arched profile and compared against those with a smooth profile. The value of the Reynolds number changed between the area of laminar flow and the one with a turbulent flow at a constant temperature of the heated surface. Research by Tauscher and Mayinger (1999) was aimed at optimising the performance of plate heat exchangers. For the visualisation of temperature fields in real time, they used the holographic interferometry method and for obtaining velocity fields, they used the Laser Doppler Anemometry method. Their experimental results were compared with numerical ones derived from computational fluid dynamics. Hartmann and Lucic (2001) presented an overview of experimental studies in the area of heat and mass transfer by means of holographic interferometry. They carried out heat transfer studies on various geometries of plate heat exchangers, drying processes, growth and condensation of bubbles during boiling. By means of two-wave

* Corresponding author, e-mail: cernecky@tuzvo.sk

holographic interferometry, they obtained simultaneously the temperature and concentration fields. The work by Herman and Kang (2002) describes research from the perspective of heat transfer intensification by adding bent blades above the edges of heated rectangular protrusions at lower values of Reynolds numbers. They visualised temperature fields by means of the holographic interferometry method. They compared the heat transfer parameters for a basic arrangement with rectangular protrusions without blades and with a smooth channel without protrusions or blades. Islamoglu and Parmaksizoglu (2003) examined the impact of the height of the gap between heat exchange surfaces on the improvement of heat transfer characteristics. They determined the heat transfer coefficient with forced air convection and a friction coefficient for a gap height of between 5 and 10 mm with a varying velocity of airflow. Naylor (2003) described the functioning principles of classical and holographic interferometry, which are used commonly for the measurement of convective heat transfer. In their work, Hwang et al. (2006) studied the nature of flow and transfer of heat and mass inside an experimental channel with a triangular profile at Reynolds numbers ranging from 100 to 5000. The local coefficients of heat and mass transfer on the channel walls were identified by using naphthalene sublimation. For an understanding of the overall flowing structure in the channel, they used the Fluent software. Isaev et al. (2010) dealt with a detailed numerical study of heat transfer enhancement by a spherical dimple placed on a wall in a narrow channel. The research was aimed at influence of the depth to diameter ratio and the Reynolds number on the flow and heat transfer. A numerical model was successfully validated using experimental measurements. Elshafei et al. (2010) dealt with experimental research on heat transfer characteristics by means of convection and pressure loss through flow in an experimental channel with arch-shaped grooves. They investigated the impact of the change of Reynolds number and the impact of the arrangement of grooves (above each other or staggered) on heat transfer and pressure loss. Lenhard et al. (2009) examined the influence of distance and height of ribs on the boundary layer in the passive roof cooling convector. Piepiorka-Stepuk and Jakubowski (2013) presented numerical simulation results determining the distributions of flow velocity and pressure in the individual channels of a plate heat exchanger. The obtained results of numerical simulations confirm the presence of inhomogeneous flow conditions in the neighbouring channels between the plates. Sajith et al. (2010) examined heat transfer by means of convection in micro channels, which are represented in various electronic sets and systems. To obtain the distribution of temperature fields, they used digital interferometry (Mach-Zehnder interferometer), whereas in the micro channel, they had water flowing. In their scientific monograph Cernecky et al. (2012) addressed the alternatives of optimising the shape of heat exchange surfaces in heat exchangers. They focused especially on experimental research of temperature fields using free and forced air convection. For a visualisation of temperature fields, they used holographic interferometry and thermal vision. They supplemented their experimental results with the results of a CFD simulation.

In this contribution, researching convective heat transfer in a set of smooth and shaped heat exchange surfaces, we used the method of holographic interferometry. The obtained local heat transfer coefficients and criterial equations for a convective heat transfer were used to determine the so-called *Colburn j-factor* in correlation with the friction coefficient *f*.

2. HOLOGRAPHIC INTERFEROMETRY

In the experiments, we used the holographic interferometry method in real time. This method enables changes of the interference image to be observed simultaneously with a change of phase non-homogeneity in real time. Initially, images of interference of an object wave ε (without phase non-homogeneity) and a reference wave ε_r (Fig. 1a) were recorded in a hologram.

After photochemical processing, the hologram will be illuminated by an object and reference beam; thus, it is possible to observe the interference of the reference wave with the object wave crossing the temperature field at the given time (Fig. 1b). The real-time method requires the intensities of the object and reference beam to be divided in order to achieve maximum contrast of the appearing fringes (Cernecky and Pivarciova, 2006).

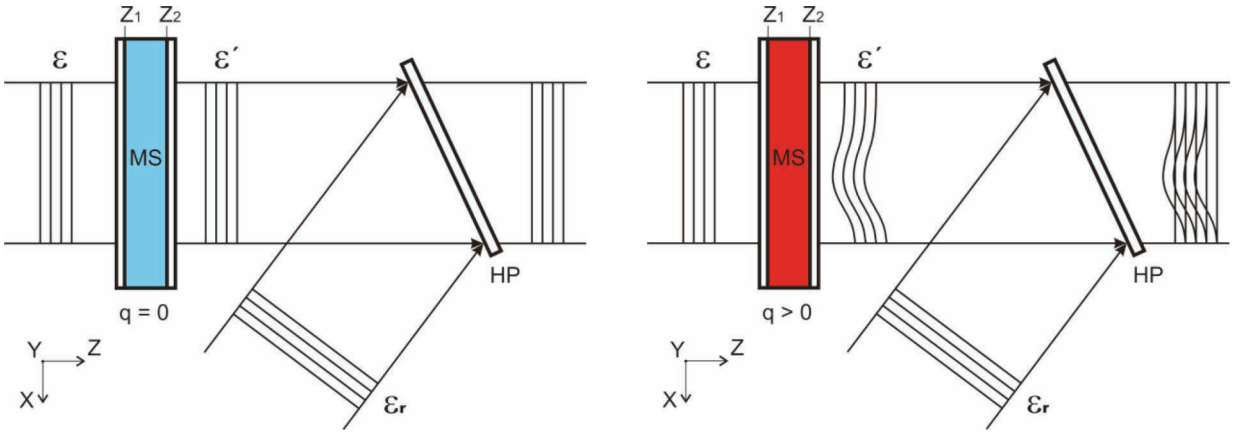

a) b)

Fig. 1. Real-time method (adjusted according to Tauscher and Mayinger, 1999).
a) records of an object and a reference wave on HD, b) reconstruction when influenced by optic nonhomogeneity
MS – measuring space, HP – holographic plate, ε – plane wave, ε´ – wave deformed by optic non-homogeneity, ε_r – reference wave

2.1. Evaluation of Holographic Interferograms

The measurable variable in interferometry is a change of the order of interference in relation to a certain reference status, i.e., the occurrence or shift of interference fringes. The occurrence or shift of interference fringes is connected with the physical changes of quantities such as density, temperature and concentration in the area monitored. In our case, we observed the temperature fields.

In an ideal interferometry case, where the optic system consists of ideal optic elements (mirrors), a monochromatic source of radiation (light) and the observation of a two-dimensional phase object without marginal effects, the change of the optic trajectory of the object beam is caused by the temperature gradient of the observed object (Manickam and Dhir, 2012).

The number of fringes appearing in the interference image, or the amount by which the interference structure is shifted as a result of the insertion of a phase object, is proportional to the phase change caused by the transit of a "light wave" through the phase object. To determine the difference in the length of optic trajectory in the case where one beam transits through the measured space, we can use the following relation (Beketova et al., 1979):

$$\Delta o = S(x,y)\cdot\lambda \tag{1}$$

In some types of interferometers, the beam may transit the measured space twice. The number of transits can be reflected by means of the constant c_i. The change of length of the optic trajectory of light is connected with the distribution of the refraction index in the monitored temperature field:

$$\Delta o = c_i \cdot \int_{z_1}^{z_2} \left[n(x,y,z) - n_f \right] dz \tag{2}$$

The order of interference may be determined according to (Manickam and Dhir, 2012; Hauf and Grigul, 1970):

$$S(x,y) = c_i \cdot \frac{1}{\lambda} \cdot \int_{z_1}^{z_2} \left[n(x,y,z) - n_f \right] dz \tag{3}$$

where $c_i = 1$ in the case of one beam transit through the phase object (e.g., in the case of a Mach-Zehnder interferometer) and $c_i = 2$ in the case of two beam transits through the phase object (e.g., in the case of a Michelson interferometer).

The relation between the refraction index and the gas density (air) is expressed by the Gladstone-Dale equation (Martynenko and Khramtsov, 2005; Vest, 1979):

$$n - 1 = K \cdot \rho \tag{4}$$

where K is the Gladstone-Dale constant, which depends on the radiation's wavelength and the gas type (air). This relation enables the switch from the distribution of the refraction index in a gas flow (air) to the distribution of density inside it.

Provided that pressure in the testing area is subject to minimum changes, i.e., it is nearly constant, the changes of density will be caused by a change of temperature. In this case, when the change of density is driven only by temperature, the distribution of temperature can be determined according to (Mayinger and Feldmann, 2000):

$$T(x,y) = \left(\frac{2S(x,y) \cdot \lambda \cdot R}{3 \cdot N \cdot W \cdot p} + \frac{1}{T_f} \right)^{-1} \tag{5}$$

Interferometric research allows efficient evaluation of heat transfer at higher temperature gradients according to the width of the thermal boundary layer, in cases where the interferometer is set at a final fringe width (Fig. 2).

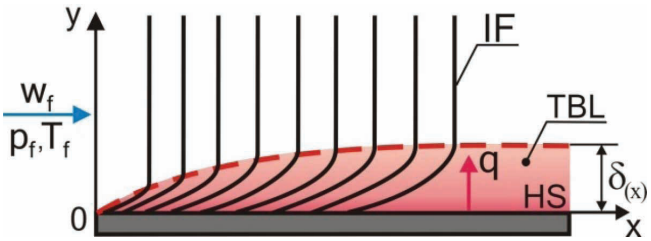

Fig. 2. Scheme of the thermal boundary layer in the case where the interferometer is set at a final fringe width. IF – interference fringe, TBL – thermal boundary layer, HS – heat exchange surface, $\delta(x)$ – width of the thermal boundary layer, q – heat flux

In case of high temperature gradients, the density of interference fringes near the wall of the heat exchange plate is high. This leads to significant deterioration in the capability of differentiating the interference fringes near the surface due to the low number of pixels forming the fringe width (Fig. 3b).

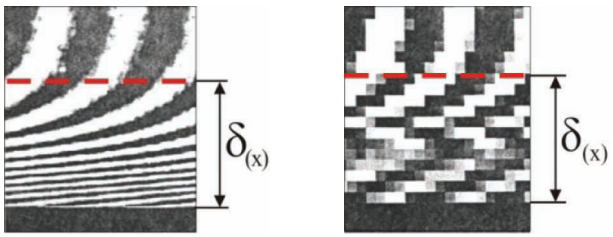

Fig. 3. Comparison of the quality of interference images of thermal boundary layers. a) quality record of an interference fringe, b) unsatisfactory quality of a record of an interference fringe

If the value of the fringe width drops below two pixels, the obtained interferogram is destroyed or lowered to the level of the shadow method. The obtained image of the temperature field interferogram is degraded and it is impossible to read the order of interference. In such cases, the heat transfer coefficient can be determined only by the width of the thermal boundary layer $\delta_{(x)}$, as illustrated in Fig. 3 (Pavelek et al., 2007):

$$\alpha_{(x)} = k\frac{\lambda_f}{\delta_{(x)}} \tag{6}$$

where λ_f is the coefficient of the fluid's thermal conductivity, k is a constant depending on the type of substitution function describing the temperature profile in the flow around the heat exchange surfaces.

In performing the experiments, the interferometer was set at an infinite width of fringes, which represented, in this case, the isotherms of the temperature field. The temperature difference between them was approximately $\Delta T = 3.8$ K. In our case, the experiments were designed so that we could calculate the heat transfer coefficient from the order of interference by means of the relation:

$$\alpha_{(x)} = -\lambda_f \left(\frac{dT}{dy}\right)_x \frac{1}{T_{s(x)} - T_f} \tag{7}$$

where $T_{s(x)}$ is the temperature of the heat exchange transfer surface in a local spot x, T_f is the temperature of the fluid and dT/dy is a derivation of temperature.

The calculation methodology and the calculation formula are incorporated in the evaluation software developed at our institution (Silaci and Cernecky, 2007). The calculation of the heat transfer coefficients, which is applied in the software, is described in more detail elsewhere (Cernecky et al., 2012).

3. EXPERIMENTAL APPARATUS

The experimental apparatus (Fig. 4) is designed for researching heat transfer between heat exchange surfaces with variable geometry, arrangement and distances, at various temperature and flow parameters with the option of expanding the apparatus by various regulating elements for the flowing air. The proposed experimental apparatus was activated in an underpressure regime and the air was sucked from the ambient environment by means of a dry lamellae air-pump. The apparatus consisted of three main areas (measuring, hydraulic and aerodynamic). The measuring area **(**MA**)** included the dismountable heat exchange surfaces (HSs) fixed at the heating plates (HP), which were made of Dural material located in the heat exchange area (HEA). The geometry of the heat exchange surfaces as well as their vertical distances and mutual arrangement could be varied. The side walls of the heat exchange area were closed by means of an optic float glass. A widened laser beam was passed through the walls for the purpose of visualising the temperature fields arising in the vicinity of the heat exchange surfaces. Fig. 4 shows an example of arched profiles arranged with surfaces without profiling above each other with vertical distance $H = 0.05$ m. The H parameter can be varied up to 0.08 m. The width of the heating plates as well as the shaped surfaces was $W = 0.2$ m and the length of the measuring section was L_2, which equals 0.4 m. The surface temperature T_s on the shaped heat exchange surfaces was measured by means of built-in temperature sensors below the heat exchange surfaces in 12 equally distributed measuring spots. The signal from the detectors was led through a connecting cable to the switch of measuring spots (SMS) and then to the Multimeter (MM). The surface temperature in the currently observed section of the heat exchange area was verified by means of a sticker K-type thermoelement (FT A683 Thermo E4, NiCr-Ni) with measurement accuracy ± 0.05 K. The temperature of the surrounding air in the room was measured by a Feuchte FHA646-1 sensor with measurement accuracy ± 0.05 K. All detectors were connected to an Almemo 2290-8 data logger. The atmospheric pressure in the room was measured by a barometer with measurement accuracy ± 50 Pa. The HEA consisted of four heating plates of equal dimensions, to which the *HSs* were fixed. Tube-shaped regulating elements were placed between the shaped surfaces with the aim of directing the flowing air inside the grooves and thereby intensifying the heat transfer process and increasing the local values of heat transfer coefficients. The difference of pressure at the input and output of the HEA was measured by means of a low-pressure detector (Huba Control 5436). The hydraulic area **(**HA**)** consisted of two thermostatic heaters (THs), which provided the heating for the heat-conducting medium (distilled water) to the required

temperature and for maintaining its set value. The heated liquid circulated from the thermostats through the tubes into the heating plates, then cooled and later it returned to the thermostats. Each heating plate had a separate hydraulic circuit. Shaped heat exchange surfaces were fixed on the heating plates by means of cylindrical head countersunk screws. The liquid in the heating plates circulated through meanders providing equal heating of the entire surface. The contact surface of the heating plate and shaped surface was covered with a heat-conductive paste for improved heat transfer between these surfaces.

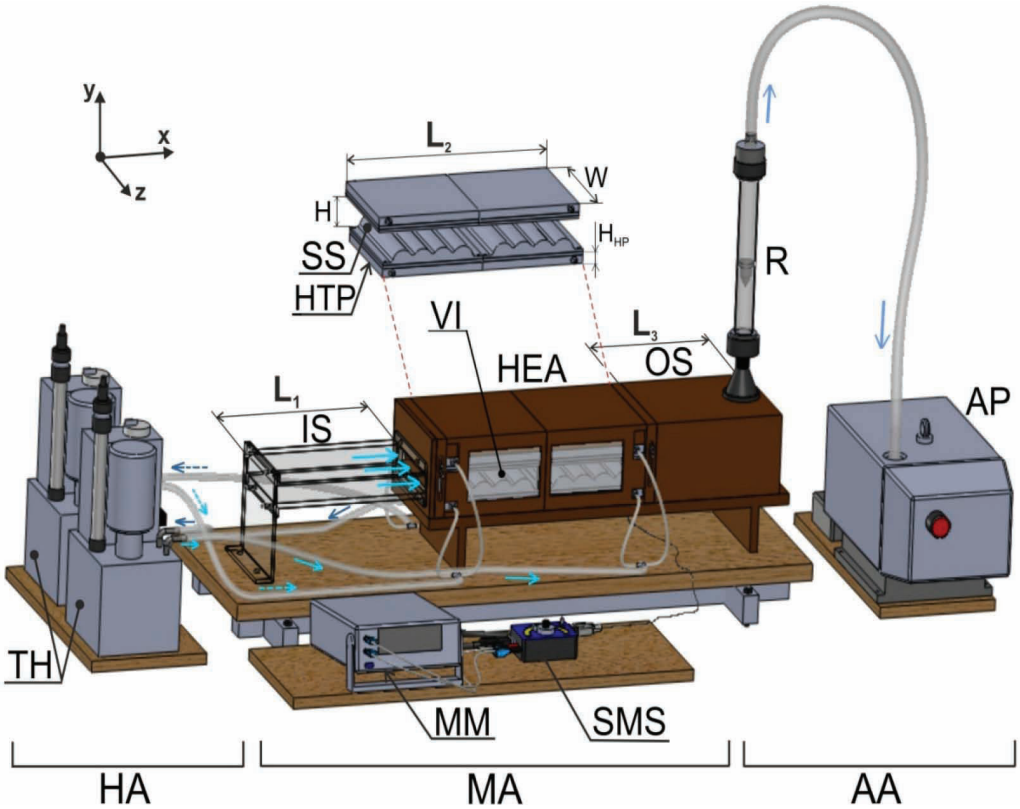

Fig. 4. Experimental apparatus activated in an under-pressure regime.
HA – hydraulic area, MA – measuring area, AA – aerodynamic area, TH – thermostatic heater, IS – input section with length L_1, HEA – heat exchange area with length L_2, OS – output section with length L_3, R – conic rotameter, AP – air-pump, MM – multimeter, SMS – switch for measuring spots, HTP – heating plate, SS – shaped heat exchange surface, H – height between heat exchange surfaces, W – width of heat exchange surfaces, VI – visors, H_{HP} – height of heating plate

The *Aerodynamic Area* **(**AA**)** consisted of a dry lamella air-pump (AP) ensuring a flow of air through the heat exchange area and of a conic rotameter (R) for measurement of the quantity of airflow with measurement accuracy ± 0.5 m^3/h. This section included an input section (IS) with length L_1 = 0.4 m providing an equal distribution and regulation of the sucked air before it entered the HEA. The output section (OS) with length L_3 = 0.25 m narrowed inside towards the rotameter.

3.1. Holographic variant of the Mach-Zehnder interferometer with an experimental apparatus setup

The temperature fields in the vicinity of the heat exchange surfaces were visualised by the method of holographic interferometry using the holographic variant of the Mach-Zehnder interferometer (Fig. 5). The holographic variant was placed on a stable holographic table (HT). The individual opto-mechanical elements are marked in Fig. 5. The experimental device (ED) (Fig. 4) was inserted in the trajectory of the object branch of the interferometer, such that the beam would pass through the examined HEA. The THs, MM, SMS and AP were all placed on separate laboratory tables (LT_1 and LT_2) to avoid vibrations on the HT, which would make it impossible to obtain a quality record of interferogram images.

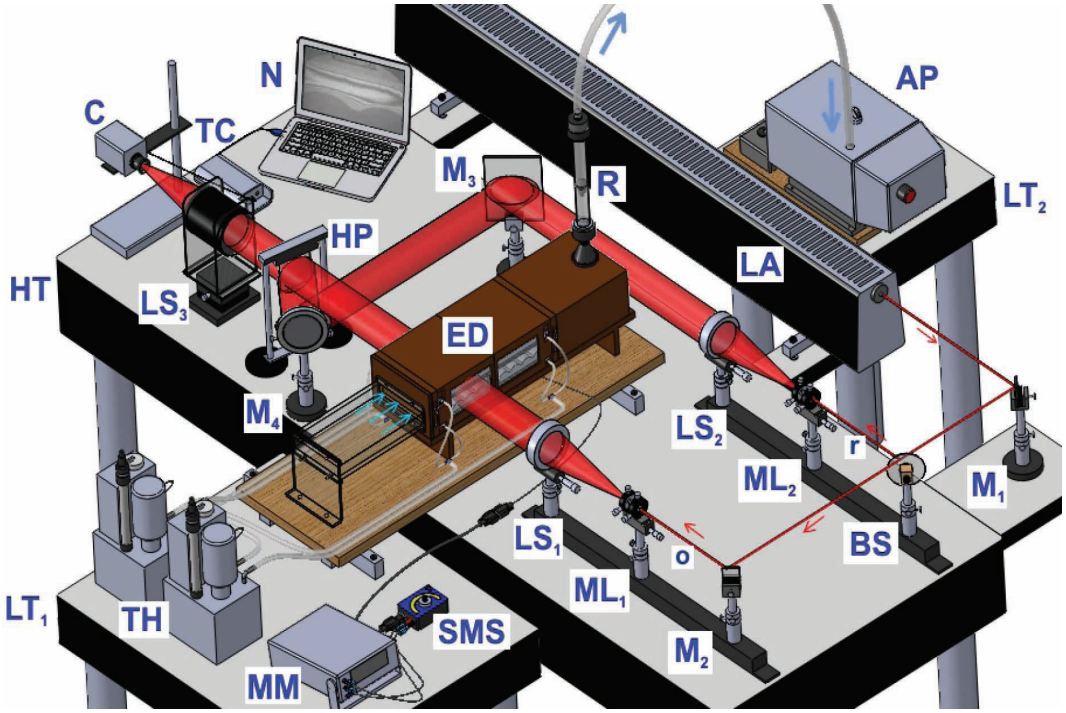

Fig. 5. Scheme of the holographic variant of the Mach-Zehnder interferometer with experimental apparatus. HT – holographic table, LT_1, LT_2 – laboratory tables, LA – He-Ne laser (λ = 633 nm), M_1 to M_4 – mirrors, BS – continual beam splitter, ML_1 and ML_2 – micro-objective lens, LS_1 to LS_3 – lenses, ED – experimental device, HP – holographic plate in a stand, C – camera, TC – television card, N – notebook, R – rotameter, AP – air-pump, TH – thermostatic heater, MM – multimeter, SMS – switch for measuring spots, o – object beam, r – reference beam

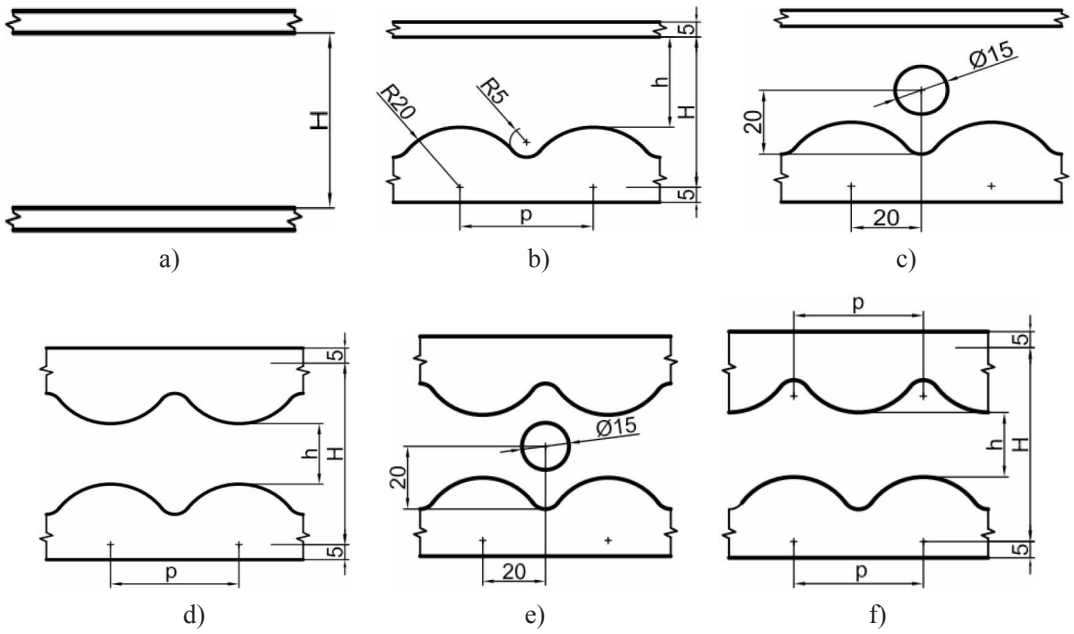

Fig. 6. Geometric parameters of the examined areas in heat exchange sets. a) arrangement A, b) arrangement B, c) arrangement C, d) arrangement D, e) arrangement E, f) arrangement F (the dimensions are given in mm)

In the experiments, we used a heat exchange set containing heated heat exchange surfaces with arched profiles. We used six various arrangements of the heat exchange surfaces (Fig. 6a to 6e), while the arrangements C and E were supplemented by regulating tubes with a diameter of 15 mm. The evaluated areas for the various geometric arrangements shown in Fig. 6 are marked by the intervals x_1 and x_2 (lower

surface) and $x_{1\cdot}$ and $x_{2\cdot}$ (upper surface) in Fig. 7. The experiments were performed at a ratio of parameters h/H = 1.0 (arrangement A), h/H =0.6 arrangements B, C) and h/H = 0.2 (arrangements D, E, F) and expressed in ratio h/p = 1.25 (arrangement A), h/p = 0.75 (arrangements B, C) and h/p = 0.25 (arrangements D, E, F).

To be able to compare the dimensionless parameters of heat transfer and pressure losses we used the Colburn j-factor and friction coefficient. The dimensionless heat transfer parameters for individual arrangements of the heat exchange sets were expressed by means of the *Colburn j-factor*, which includes the qualities of the flowing air (kinematic viscosity, density etc.) and its velocity at the given flow cross section of the set and also the value $\alpha_{(x)}$ along the heat exchange surfaces (Islamoglu and Parmaksizoglu, 2003):

$$j = \frac{Nu_m}{Re \cdot Pr^{1/3}} \tag{8}$$

$$Nu_m = \frac{\alpha_m \cdot D_h}{\lambda_f} \tag{9}$$

The Reynolds criterion was calculated according to the relation (Herman and Kang, 2001):

$$Re = \frac{w_f \cdot D_h}{v} \tag{10}$$

$$D_h = \frac{4 \cdot W \cdot H}{2\left(W + H\right)} \tag{11}$$

where D_h is the hydraulic diameter of the channel, the width of which was W = 0.2 m and height H_m in the case of the shaped surfaces was considered based on the relation $H_m = (H+h)/2$. Because the physical parameters of the air in the examined area were not changed significantly, the value Pr can be considered constant (Pr = 0.71) and it was calculated according to the following relation:

$$Pr = \frac{v \cdot \rho \cdot c_p}{\lambda_f} \tag{12}$$

where the physical parameters for air with temperature of 296.15 K and atmospheric pressure 100,200 Pa were determined based on the literature (Pavelek et al., 2007).

As the shapes of the heat exchange surfaces themselves (or the inserted regulating elements) cause an increase of pressure loss, it was also necessary to determine the friction coefficient values. The friction coefficient was calculated based on the relation for the entire heat exchange area with length L_2 = 0.4 m (Fig. 4) at an airflow rate Q = 20 m^3/h (Herman and Kang, 2002):

$$f = \frac{\Delta p}{\frac{L_2}{D_h} \cdot \frac{\rho \cdot w_{f,m}^2}{2}} \tag{13}$$

where $w_{f,m}$ is the mean velocity of the flowing fluid (air).

4. RESULTS AND DISCUSSION

In the experiments, using the holographic interferometry method, we obtained images of the temperature fields in the heat exchange sets with geometrical arrangements A to F, which are shown in Fig. 7. From the obtained images of the holographic interferograms, we determined the local heat transfer coefficients based on the mean heat transfer parameters for airflow quantities ranging from 5 to 20 m^3/h.

Fig. 7a shows the set A with heat exchange surfaces without profiling. In the flow direction, we identified a gradual increase in the width of the thermal boundary layer, leading to an increase of the thermal resistance and to the value of the *Colburn j-factor* attaining the lowest value within the sets examined ($j = 0.0078$).

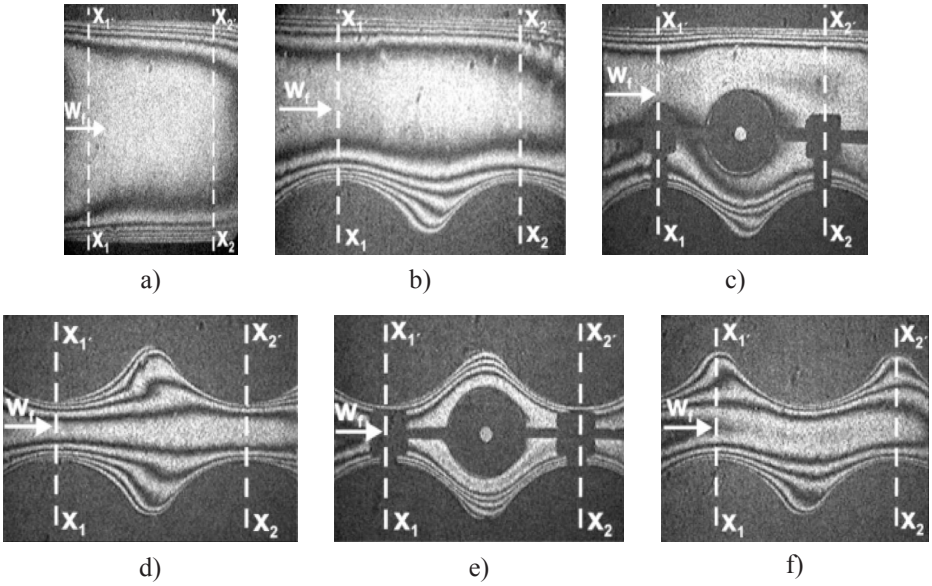

Fig. 7. Images of holographic interferograms of heat exchange sets with geometrical arrangements A to F for $H = 0.05$ m and $Q = 20$ m^3.h^{-1}

Additionally, the pressure losses attained the lowest values ($f = 0.3584$), because in this case, the surface friction was the lowest with no obstacles (tubes) inserted into the airflow trajectory. For the purposes of improving the heat transfer parameters, on the bottom surface we placed a shaped heat exchange surface with an arched profile (Fig. 7b). The shaped profile caused an increase of the mean heat transfer parameters but also that of pressure losses, which can be observed in the *j* and *f* factors shown in Fig. 8. Fig. 7c shows the image of a temperature field in set C with a regulating tube. Compared with the tube-less set, the *j* and *f* factors recorded an increase.

Based on Fig. 7d, we can state that in the narrowed space, the width of the thermal boundary layers diminished. The extended part of the space shows an increase of the widths of thermal boundary layers and consequently, an increase of thermal resistance. From the point of view of mean heat transfer parameters and the friction coefficient (*j* and *f*), these also increased compared with sets A to C. For the purposes of intensifying the heat transfer, we placed regulating tubes between the profiled surfaces to reduce the thermal resistance. This led to an increase of the heat transfer parameters ($j = 0.0226$) and this set reached the highest values of mean heat transfer parameters but also the highest pressure losses ($f = 28.482$). By inserting the regulating tubes in the extended space of the heat transfer set E (Fig. 7e), the width of the thermal boundary layer was reduced. This resulted in an increase of the local heat transfer coefficients. In the case of a staggered arrangement of the arched profiles (Fig. 7f), the *j* and *f* values were higher compared with the set of arches arranged directly above each other (set D).

The analysis of heat exchange sets (arrangements A to F) shows that the regulating tubes inserted between the heat exchange sets with arrangements C and E caused an increase of the local heat transfer coefficients and thereby, also caused an increase of the mean *Nu* values (Fig. 8).

In the set with arrangement E with height $H = 0.05$ m, we can observe a significant increase of the mean *Nu* values, e.g., at the flow rate $Q = 20$ m^3/h, up to the value of 38.26. Regulation of the airflow inside the arched grooves drives a more intense heat transfer. Therefore, set E reaches the highest values of mean *Nu* with the height of the gap at 0.05 m (from 36.7 to 38.3). From the perspective of the simultaneous evaluation of heat transfer parameters and pressure loss, sets without regulating tubes are more efficient.

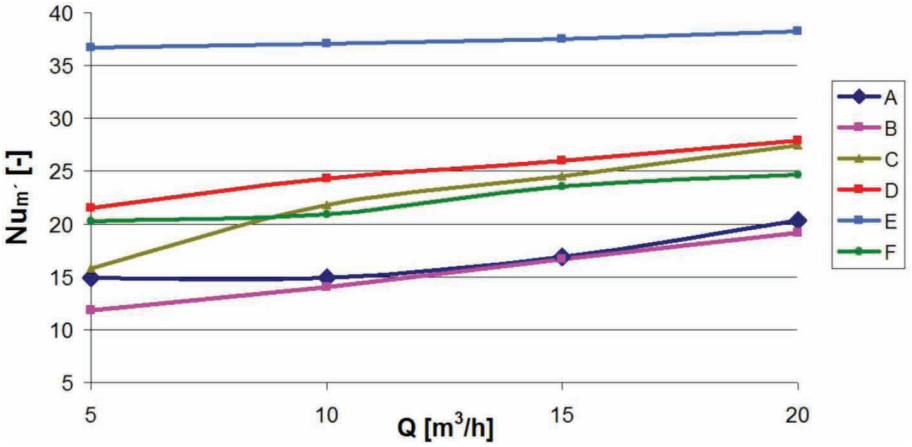

Fig. 8. Comparison of heat exchange sets A to F from the perspective of heat transfer for $H = 0.05$ m.

The placement of arched profiles above each other (set D) leads to higher mean *Nu* values. For mutual comparison of the individual shapes, we used the height *h*, i.e., the height between the tops of the protrusion and the upper flat surface and/or between the tops of the protrusions.

The resulting values of the *Colburn j-factor* and the *friction coefficient f* for individual heat exchange sets with airflow of 20 m^3/h are specified in Table 1.

Graphic comparisons of heat exchange sets A to F from the perspective of heat transfer parameters and simultaneous pressure loss are shown in Fig. 9.

Table1. Values of *j* and *f* factors achieved in heat transfer sets A to F for $H = 0.05$ m and airflow rate $Q = 20$ m^3/h

	Geometrical arrangement					
	A	B	C	D	E	F
j [-]	0.78×10^{-2}	0.88×10^{-2}	1.26×10^{-2}	1.65×10^{-2}	2.26×10^{-2}	1.46×10^{-2}
f [-]	0.358	1.029	4.912	8.720	28.482	6.192

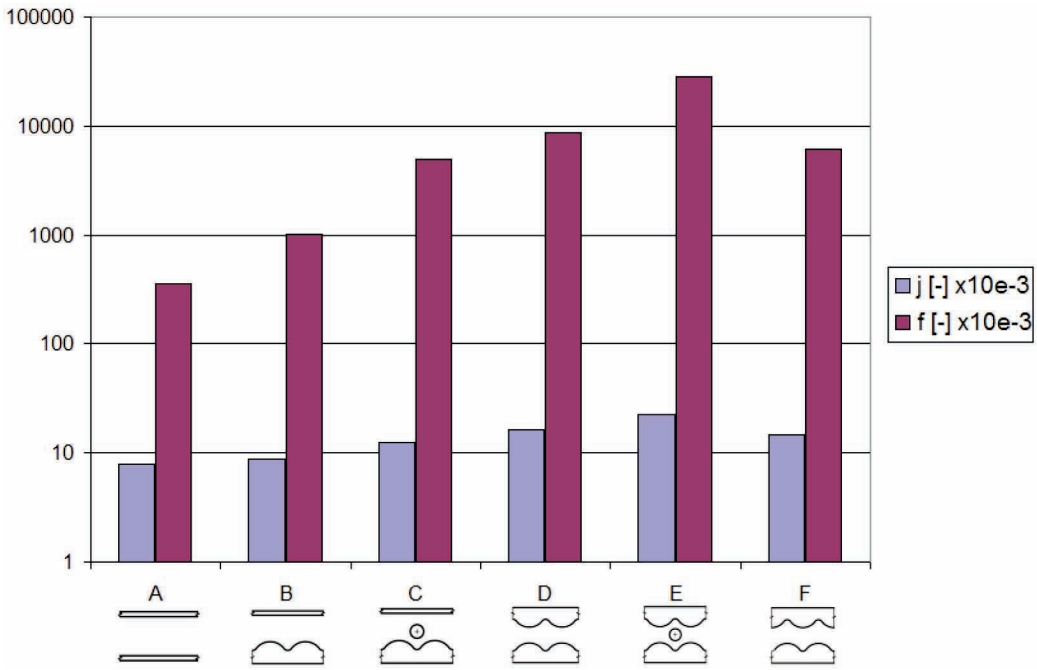

Fig. 9. Comparison of heat exchange sets from the perspective of heat transfer and pressure loss for geometrical arrangements A to F, $H = 0.05$ m, $Q = 20$ m^3/h

5. CONCLUSION

Holographic interferometry was used to experimentally examine the temperature fields and subsequently determine the heat transfer parameters in an experimental channel consisting of a heat exchange set with various geometrical arrangements. Six geometrical arrangements of heat exchange surfaces consisting of surfaces with arched profiles, flat surfaces and arrangements with regulating tubes were considered for a range of Re values from 476 to 2926.

Heat transfer intensification can be reached at low *Re* values by means of a suitable geometrical arrangement of the heat exchange surfaces. From the perspective of the mean heat transfer parameters, the highest values were achieved for the case of an arrangement of arched profiles with regulating tubes (arrangement E). However, this set also recorded the highest pressure losses, which exceeded pressure losses in the other sets considerably. The lowest pressure losses were attained by heat exchange sets containing smooth surfaces without protrusions (arrangement A). This arrangement has characteristics of a gradual increase of the thermal boundary layer, which causes a reduction of the heat transfer parameters.

With increasing ratios of h/H and h/p, the mean heat transfer parameters fall, as do the pressure losses. The research results show that by using profiled heat exchange surfaces and by inserting regulating tubes, the process of heat transfer is intensified but at the same time, the pressure losses increase. By using profiled heat exchange surfaces, the pressure losses increase, which being intensified by the insertion of regulating tubes. Therefore, because of this, it is important to examine pressure losses as well as heat transfer parameters in heat exchange sets.

This contribution was created within the Cultural and Educational Grant Agency, project No. 044SPU-4/2014 funded by the Ministry of Education, Science, Research and Sport of the Slovak Republic.

SYMBOLS

c	specific heat capacity, J/(kg×K)
c_i	constant,
D	diameter, m
ED	experimental device
f	friction coefficient,
H, h	height, m
j	Colburn factor,
K	Gladstone-Dale constant, m^3/kg
k	constant,
L	length, m
N	molar refractivity, m^3/mol
Nu	Nusselt number,
n	refractive index,
OS	output section
o	object beam
Pr	Prandtl number,
p	pressure, Pa
p	spacing, m
Q	flow rate, m^3/h
q	heat flow density, W/m^2
R	radius, m
R	gas constant, J/(kg×K)

r	reference beam
Re	Reynolds number,
S	interference order,
T	temperature, K
W	width of heat exchange surfaces, m
w	velocity, m/s
x, y, z	coordinate system axes

Greek symbols

α	heat transfer coefficient, W/(m^2×K)
δ	thickness of thermal boundary layer, m
Δo	optical path change, m
Δp	pressure difference, Pa
ΔT	temperature difference, K
ε	plane wave,
ε'	wave deformed by optic non-homogeneity,
ν	kinematic viscosity, m^2/s
ø	diameter, m
λ	thermal conductivity coefficient, W/(m×K)
λ	wavelength of light, m
ρ	density, kg/m^3

Subscripts

1, 2, 3	sequence
f	fluid
h	hydraulic
m	mean value
p	pressure
r	reference
s	surface
(*x*)	local value

Abbreviations

AA	aerodynamic area
AP	air-pump
BS	beam splitter
C	camera
CFD	Computational Fluid Dynamics
HA	hydraulic area
HEA	heat exchange area
HTP	heating plate
HS	heat exchange surface
HP	holographic plate
HP	heating plate
HT	holographic table
IF	interference fringe
IS	input section
LS	lens
LA	laser
LT	laboratory table
MA	measuring area
ML	micro-objective lens

M	mirror
MM	multimeter
MS	measuring space
N	notebook
R	conical rotameter
SMS	switch for measuring spots
SS	shaped heat exchange surface
TBL	thermal boundary layer
TC	television card
TH	thermostatic heaters
VI	visors

REFERENCES

Beketova A.K., Belozerov A.F., Berezkin A.N., 1979. *Gologaficheskaya interfrometriya fazovykh ob´ektov/ Holografická interferometria fázových objektov*. Izdateľstvo Nauka (in Russian).

Cernecky J., Koniar J., Brodnianska Z., 2012. *Možnosti optimalizácie tvaru teplovýmenných plôch výmenníkov tepla s využitím experimentálnych metód a fyzikálneho modelovania*. Vedecká monografia. Zvolen: Vydavateľstvo TU vo Zvolene (in Slovak).

Cernecky J., Pivarciova E., 2006. *Possibilities and prospects of holography.* Russia: Izhevsk State Technical University.

Elshafei E.A.M., Awad M.M., Negiry E., Ali A.G., 2010. Heat transfer and pressure drop in corrugated channels. *Energy*, 35, 101-110. DOI: 10.1016/j.energy.2009.08.031.

Hartmann A., Lucic A., 2001. Application of the holographic interferometry in transport phenomena studies. *Heat Mass Transfer*, 37, 549 – 562. DOI: 10.1007/s002310100237.

Hauf W., Grigull V., 1970. *Optical methods in heat transfer, advances in heat transfer.* London, Academie Press.

Herman C., Kang E., 2001. Experimental visualization of temperature fields and study of heat transfer enhancement in oscillatory flow in a grooved channel. *Heat Mass Transfer*, 37, 87-99. DOI: 10.1007/s002310000101.

Herman C., Kang E., 2002. Heat transfer enhancement in a grooved channel with curved vanes. *Int. J. Heat Mass Transfer*, 45, 3741-3757. DOI: 10.1016/S0017-9310(02)00092-3.

Hwang S.D., Jang I.H., Cho H.H., 2006. Experimental study on flow and local heat/mass transfer characteristics inside corrugated duct. *Int. J. Heat Fluid Flow,* 27, 21-32. DOI: 10.1016/j.ijheatfluidflow.2005.07.001.

Isaev S.A., Kornev N.V., Leontiev A.I., Hassel E., 2010. Influence of the Reynolds number and the spherical dimple depth on turbulent heat transfer and hydraulic loss in a narrow channel. *Int. J. Heat Mass Transfer,* 53, 178–197. DOI: 10.1016/j.ijheatmasstransfer.2009.09.042.

Islamoglu Y., Parmaksizoglu C., 2003. The effect of channel height on the enhanced heat transfer characteristics in a corrugated heat exchanger channel. *Appl. Therm. Eng.,* 23, 979-987. DOI: 10.1016/S1359-4311(03)00029-2.

Kilicaslan I., Sarac H.I., 1998. Enhancement of heat transfer in compact heat exchanger by different type of rib with holographic interferometry. *Exp. Therm. Fluid Sci.,* 17, 339-346. DOI: 10.1016/S0894-1777(98)00006-5.

Lenhard R., Jandacka J., Malcho M., 2009. Influence of distance and height ribs on boundary layer in to the passive roof cooling convector. *Acta Metall. Slovaca*, 15, 168-173.

Manickam S., Dhir V., 2012. Holographic interferometric study of heat transfer to a sliding vapor bubble. *Int. J. Heat Mass Transf.*, 55, 925 – 940. DOI: 10.1016/j.ijheatmasstransfer.2011.10.016.

Martynenko O.G., Khramtsov P.P., 2005. *Free-convective heat transfer.* Springer Verlag, Berlin.

Mayinger F., Feldmann O., 2000. *Optical measurements, techniques and applications, heat and mass transfer.* Springer, Berlin, Germany.

Naylor D., 2003. Recent developments in the measurement of convective heat transfer rates by laser interferometry. *Int. J. Heat Fluid Flow,* 24, 345-355. DOI: 10.1016/S0142-727X(03)00021-3.

Pavelek, M., Janotkova, E., Stetina, J., 2007. *Vizualizační a optické měřicí metody*. 2nd edition. Vysoké učení technické v Brně, Brno (in Czech).

Piepiorka-Stepuk J., Jakubowski M., 2013. Numerical studies of fluid flow in flat, narrow-gap channels simulating plate heat exchanger. *Chem. Process Eng*., 34, 507–514. DOI: 10.2478/cpe-2013-0041.

Sajith V., Haridas D., Sobhan C.B., Reddy G.R.C., 2010. Convective heat transfer studies in macro and mini channels using digital interferometry. *Int. J. Therm. Sci.,* 50, 239-249. DOI: 10.1016/j.ijthermalsci.2010.04.005.

Silaci J., Cernecky J., 2007. *Manuál ku softvéru Vibra 2a pre vyhodnocovanie holografických interferogramov.* Technická univerzita vo Zvolene, Zvolen, Slovenská Republika (in Slovak).

Tauscher R., Mayinger F., 1999. Visualization of flow temperature fields by holographic interferometry – Optimization of compact heat exchangers. *2nd Pacific Symposium on Flow Visualization and Image Processing*. Honolulu, USA, 16-19 May 1999.

Vest Ch.M., 1979. *Holographic interferometry*. New York, John Wiley.

Received 18 July 2014
Received in revised form 05 May 2015
Accepted 25 July 2015